

Chiral Surface Plasmon Polaritons on Metallic Nanowires

Shunping Zhang,¹ Hong Wei,¹ Kui Bao,² Ulf Håkanson,^{1,4} Naomi J. Halas,^{1,2,3}
Peter Nordlander,^{1,2} and Hongxing Xu^{1,4,*}

¹*Beijing National Laboratory for Condensed Matter Physics and Institute of Physics,
Chinese Academy of Sciences, Beijing 100190, China*

²*Department of Physics and Astronomy, Laboratory for Nanophotonics, Rice University, Houston, Texas 77005, USA*

³*Department of Electrical and Computer Engineering, Rice University, Houston, Texas 77005, USA*

⁴*Division of Solid State Physics/The Nanometer Structure Consortium, Lund University, Lund, Sweden*

(Received 28 April 2011; revised manuscript received 16 June 2011; published 23 August 2011)

Chiral surface plasmon polaritons (SPPs) can be generated by linearly polarized light incident at the end of a nanowire, exciting a coherent superposition of three specific nanowire waveguide modes. Images of chiral SPPs on individual nanowires obtained from quantum dot fluorescence excited by the SPP evanescent field reveal the chirality predicted in our theoretical model. The handedness and spatial extent of the helical periods of the chiral SPPs depend on the input polarization angle and nanowire diameter as well as the dielectric environment. Chirality is preserved in the free-space output wave, making a metallic nanowire a broad bandwidth subwavelength source of circular polarized photons.

DOI: 10.1103/PhysRevLett.107.096801

PACS numbers: 73.20.Mf, 42.25.Ja, 78.67.Uh

The interaction of circularly polarized electromagnetic fields with chiral objects, such as chiral molecules, is a topic of fundamental interest, which also has important applications in fields such as molecular spectroscopy and structural biology [1,2]. Recent advances in our understanding of how to shape electromagnetic fields at nano-scale dimensions have led to the concept of tailoring the optical chirality to match molecular dimensions, and to the design and demonstration of chiral metamaterials [3]. Metallic structures play an important role in addressing this challenge, since they support surface plasmon polaritons (SPPs), which are collective excitations of their conduction electrons. SPPs enable localized and highly spatially structured electromagnetic fields that can be scaled down to nanometer dimensions [4].

Single crystalline metallic nanowires have recently attracted significant interest as subwavelength SPP waveguides, analogs of optical fiber waveguides but with nanometer-scale cross sections and micron-scale propagation lengths. The strong coupling between proximal quantum emitters and nanowire SPPs, facilitated by the small mode volume, enables nanowires to serve as quantum information transmission lines [5,6]. Nanowires can function as low- Q Fabry-Pérot resonators [7] and as unidirectional subwavelength light sources [8], by exciting SPPs with light incident at a nanowire terminus. Active control of the phase or polarization state of the incident excitation can generate coherent superpositions of nanowire SPPs, creating a series of nanowire-based plasmonic devices, such as routers, modulators, even all-optical Boolean logic gates that can perform simple computational operations [9,10]. In this Letter, we show that chiral SPPs can be generated on metallic nanowires by exciting a superposition of nanowire SPP modes. The chirality of the guided

SPPs is preserved in the emitted photon at the distal end, enabling the nanowire to function as a subwavelength circularly polarized light source.

For an infinitely long metallic nanowire, the SPPs can be modeled analytically [6,11,12]. In cylindrical coordinates, the electric field takes the form $\mathbf{E}^j(\mathbf{r}) = \sum_m a_m^j \mathbf{E}_m^j(k_{m,\perp}^j \rho) e^{im\phi} e^{ik_{m,\parallel}x}$, where the superscript $j = D, M$ represents the region outside (dielectric) and inside (metal) the wire, respectively, and m is the azimuthal quantum number. a_m^j and $k_{m,\parallel}$ are the amplitude and the propagating constant of the m th mode, respectively, and (ρ, ϕ, x) are the cylindrical coordinates. $k_{m,\parallel}$ is related to the transverse wave vector $k_{m,\perp}^j$ by $k_{m,\parallel}^2 + k_{m,\perp}^{j2} = \epsilon^j k_0^2$, where ϵ^j is the dielectric constant in region j and k_0 is the wave number in vacuum. The TM_0 ($m = 0$) mode is a no-cutoff, axially symmetric mode resulting from electrons oscillating parallel to the wire axis. The two degenerate first order modes, HE_{-1} ($m = -1$) and HE_1 ($m = 1$), correspond to charge oscillations in the vertical and horizontal plane, respectively. These two modes exhibit an exponential growth of their mode volume in the thin wire limit [6].

For a finite length wire, local symmetry-breaking at the wire terminus is sufficient to allow the SPPs to be excited by incident light via mode matching. The excitation geometry is depicted in Fig. 1(a) and is modeled using finite element method (COMSOL Multiphysics 3.5a, RF Module). Optical constants for Ag are interpolated from Ref. [13]. The incident excitation is described by a paraxial Gaussian beam (waist $w_0 = 1.0 \mu\text{m}$) with an instantaneous electric field of the form $\mathbf{E}_{\text{inc}}(\mathbf{r}) = \mathbf{E}_0(\mathbf{r})e^{-i\varphi}$, where $\varphi = \omega t$ is the incident phase and $\mathbf{E}_0(\mathbf{r})$ is the mode profile of the incident light. For optically “thick” nanowires where retardation

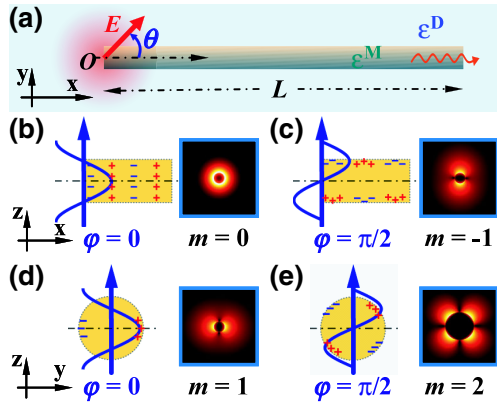


FIG. 1 (color online). (a) Schematic illustration of the nanowire in homogeneous background. The incident Gaussian beam with an electric field \mathbf{E} and a polarization angle θ is focused normally on the left nanowire end. ϵ^M and L are the permittivity and the length of the Ag nanowire, respectively. Excitation of the (b) $m = 0$ (TM_0) and (c) $m = -1$ (HE_{-1}) mode at an incident phase $\varphi = 0$ and $\varphi = \pi/2$, respectively, for $\theta = 0^\circ$. Excitation of the (d) $m = 1$ (HE_1) and (e) $m = 2$ (HE_2) mode at $\varphi = 0$ and $\varphi = \pi/2$, respectively, for $\theta = 90^\circ$. The electric field $|\mathbf{E}|$ profile of each excited SPP mode is shown on the right in panels (b)–(e). The radius R of the simulated Ag nanowire is 60 nm in (b–d) and 250 nm in (e). The permittivity of the embedding medium ϵ^D is 2.25 and the incident wavelength λ_0 is 632.8 nm in vacuum, same as in the following figures.

effects are significant, several plasmonic modes can be excited simultaneously by the incident light with an appropriate polarization at the wire terminus [Figs. 1(b)–1(e)] [14]. For $\varphi = 0$, selective excitation of the TM_0 or HE_1 mode is achieved by aligning the incident polarization parallel ($\theta = 0^\circ$) or perpendicular ($\theta = 90^\circ$) to the wire axis, as illustrated in Figs. 1(b) and 1(d), respectively. With a $\pi/2$ phase shift of φ , the local field profile across the nanowire terminus changes in symmetry creating an electric field that is antisymmetric across the $z = 0$ plane. The excitation profile now matches the mode distribution of HE_{-1} [Fig. 1(c)] or HE_2 [Fig. 1(e)] for $\theta = 0^\circ$ or $\theta = 90^\circ$, respectively. Therefore, for an arbitrary input phase φ , both TM_0 and HE_{-1} modes are excited for $\theta = 0^\circ$, and both HE_1 and HE_2 modes are excited for $\theta = 90^\circ$. Experimentally we should see the cycle-averaged superposition of all excited modes, with amplitudes dependent on the ratio of nanowire diameter to the wavelength of incident light.

For $0^\circ < \theta < 90^\circ$, the three lowest modes ($|m| \leq 1$) are excited simultaneously, but in a manner such that the HE_{-1} mode has a constant phase delay $\Delta\Phi = \pi/2$ with respect to the HE_1 mode. A full range of elliptical SPPs can be generated in this manner. The coherent interference of these two SPP waves of equal amplitude results in a circularly polarized guided wave, characterized by its circular angular momentum σ_\pm , in direct analogy with photons. The contribution of the simultaneously excited

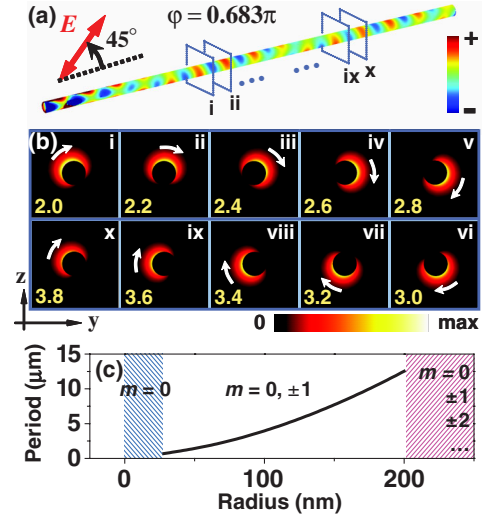


FIG. 2 (color online). Chiral SPPs. (a) Surface charge density plot on a Ag nanowire. The maximal value of surface charge was truncated at the incident end to better show the plasmon modes on the wire. (b) Time-averaged power flow in the yz plane at different positions along the nanowire, where $x = 2.0$ to $3.8 \mu\text{m}$ (i–x) in steps of $0.2 \mu\text{m}$, indicated by the blue frames in (a). The white arrows highlight the rotation of electromagnetic energy as a function of position along metal nanowire, showing right-handed chiral SPPs. (c) Periods of the plasmon helix, Λ , as a function of nanowire radius. The blue region denotes the single mode-dominant regime and the magenta region denotes the multimode regime. The length of the simulated nanowire ($R = 60 \text{ nm}$) is $L = 5.0 \mu\text{m}$ and the incident polarization angle is $\theta = 45^\circ$ in (a),(b).

TM_0 mode is to stretch the circularly polarized SPP into a helical wave, with a spiral near-field pattern. For a given nanowire cross section, the circularly polarized SPP, with its varying temporal electron oscillations interferes with the TM_0 mode constructively on one side of the nanowire but destructively on the other side. Figure 2(a) shows a typical surface charge distribution of a chiral SPP on a nanowire ($R = 60 \text{ nm}$) locally excited by a Gaussian beam with incident phase $\varphi = 0.683\pi$ and polarization angle $\theta = 45^\circ$ [15]. A helical propagating SPP resulting from the superposition of the three lowest SPP modes is clearly observed. The time-averaged power flow at various cross sectional positions of the nanowire, shown in Fig. 2(b), further confirms this helical behavior. As indicated by the white arrow, the electromagnetic energy revolves around the metal-dielectric interface as the SPP propagates along the nanowire. In the example shown here, the period of the helix (Λ) is about $1.83 \mu\text{m}$.

The handedness of the chiral SPP is determined by the phase delay between the HE_1 and HE_{-1} modes. An advanced phase for the HE_1 mode relative to the HE_{-1} mode corresponds to a clockwise rotation of the collective electron motion as viewed in the direction of propagation, resulting in a right-handed SPP $|\sigma_+ = 1\rangle$. The converse is true for a left-handed SPP $|\sigma_- = -1\rangle$ which can be

excited by rotating θ to $-\theta$. The relative amplitudes of the HE_1 and HE_{-1} modes are proportional to the perpendicular and parallel components of the incident beam with respect to the nanowire axis; hence, a direct tailoring of circularly or elliptically polarized SPPs can be achieved simply by varying θ . In this way, a controllable spatial distribution of the surface plasmon energy can be achieved. For parallel excitation, the HE_1 mode will not be excited, resulting in a conversion of the helical characteristic of the guided wave into a spatially dependent interference, or “beat”, between the remaining excited plasmons.

The period of a chiral SPP is proportional to the inverse of the difference between the propagation constants of the TM_0 and HE_1 (or TM_0 and HE_{-1}) mode: $\Lambda = 2\pi(\text{Re}(k_{0,\parallel} - k_{1,\parallel}))^{-1}$. By solving the transcendental equation numerically [6], the period of a chiral SPP on a Ag nanowire as a function of wire radius is obtained [Fig. 2(c)]. For increasing nanowire radius, the propagation constant of the TM_0 mode decreases and that of the HE_1 mode increases [12], yielding a larger helical period. Since phase retardation is critical to the formation of a chiral SPP, the size of the nanowire must be comparable to the excitation wavelength $R \sim \lambda_0/\sqrt{\epsilon^D}$. For very thin nanowires ($R \ll \lambda_0/\sqrt{\epsilon^D}$), the helices (and also the “beats”) disappear because the structure will only support $m = 0$ modes. For larger wires, the excitation of higher order modes ($|m| \geq 2$) results in complicated field distributions that countermand the chirality of SPPs. Therefore, the chiral SPPs we report here appear between these two regimes. In addition to the diameter of the nanowire, its material composition, embedding medium and excitation wavelength will all affect the excitation of chiral SPPs. We note that the chiral SPPs are not eigenmodes of the system but linear combinations of the principal eigenmodes ($m = 0, \pm 1$). The different amplitudes and phases imparted on these eigenmodes by the excitation source will determine their pitch and handedness.

Chiral SPPs were directly observed experimentally by means of quantum dot-based fluorescence imaging of the nanowire evanescent field [10]. Ag nanowires (about 150 nm in radius) were deposited on a glass substrate, followed by a 10 nm alumina oxide coating to prevent quenching of the subsequently deposited quantum dots. Here it was found that a homogeneous dielectric embedding medium for the nanowire was critical for the observation of chiral SPPs. This was achieved using index-matching oil to preserve the cylindrical symmetry of the system. A set of fluorescent images obtained in this manner are shown in Fig. 3. The helical near-field is clearly resolved when the incident polarization is oriented at 45° (ii) or -45° (iii) to the wire axis. The handedness of the helix is reversed by rotating the polarization from 45° to -45° . The measured helix period is $7.3 \mu\text{m}$, in good agreement with $7.7 \mu\text{m}$ from theoretical calculations in Fig. 2(c) for $R = 150 \text{ nm}$. The helical field pattern

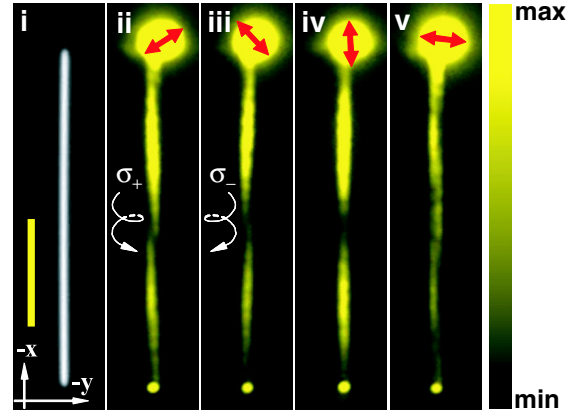


FIG. 3 (color online). (i) Optical image of a Ag nanowire. The scale bar is $5 \mu\text{m}$. (ii),(iii) Fluorescence images of right-handed (ii) and left-handed (iii) SPPs, respectively. The white helical arrows highlight the handedness of the plasmon helix. (iv),(v) SPPs launched with incident polarization (iv) parallel and (v) perpendicular to the nanowire axis show suppression of the plasmon helix. All images (ii-v) are obtained by quantum dot imaging, with He-Ne laser excitation (632.8 nm).

disappears when the polarization is parallel (iv) or perpendicular (v) to the nanowire, also in agreement with our theoretical analysis. The residual plasmon beat appearing in (v) may be caused by asymmetries in the excitation beam and/or the shape of the wire end, allowing TM_0 mode excitation for perpendicular incident polarization.

A direct consequence of the generation of chiral SPPs is the chirality of the emission light at the nanowire output. The degree of circular polarization C [16] for this structure is defined with slight modification to take the longitudinal field components into account:

$$C = \frac{2\langle E_y(t)E_z(t)\sin(\delta_y - \delta_z) \rangle}{\langle E_x^2(t) \rangle + \langle E_y^2(t) \rangle + \langle E_z^2(t) \rangle}, \quad (1)$$

where $\langle \rangle$ denotes time average, and $\delta_y - \delta_z$ is the phase difference between the two transverse electric field components E_y and E_z . The relative intensity is $I = |\mathbf{E}(\mathbf{r})|^2/|\mathbf{E}_0(0)|^2$, where $\mathbf{E}_0(0)$ represents the incident electric field at the origin. Figure 4(a) shows a spatial map of C in a vertical plane 200 nm beyond the output end of the nanowire. As expected, the emitted photon preserves the chirality of the SPP. Despite the presence of a nonzero longitudinal field component, a high degree of circular polarization ($C \sim 0.90$) is obtained. The figure of merit $f = I \times C^2$, shown in Fig. 4(b), further confirms the high degree of circular polarization of the outgoing optical wave. The ellipticity of the polarization state of the emitted photon can be tuned in a continuous fashion by rotating the incident polarization angle θ [Fig. 4(c)]. Higher C appears around $\theta = 45^\circ$, when the HE_1 and HE_{-1} modes have nearly equal amplitudes. Unlike conventional quarter-wave plates or resonance-based subdiffraction circularly polarized sources [16], metallic nanowires

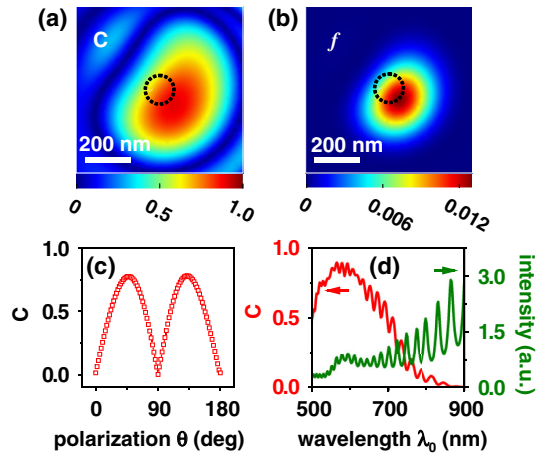


FIG. 4 (color online). Maps of degree of circular polarization C (a) and figure of merit f (b) in a vertical plane 200 nm beyond the distal end of the nanowire in Fig. 2. The black dotted circles indicate the cross section of the nanowire. C at the center of (a) on the symmetric axis of the nanowire as a function of θ (c) and λ_0 (d). The transmission spectrum $I(\lambda_0)$ (green) is also shown in (d).

support a continuum of SPPs, making this geometry ideal as a broadband source of circularly polarized light. Figure 4(d) shows that photons emitted from the nanowire maintain a high C (> 0.50) over a wide wavelength window, spanning most of the visible region of the spectrum. The modulations appearing in $C(\lambda_0)$ (red) are due to etaloning in the nanowire and also appear in the transmission spectrum $I(\lambda_0)$ at the nanowire output (green). The anticorrelation between C and I at longer wavelengths (> 610 nm), shown in Fig. 4(d), is caused by the dominance of the longitudinal field component E_x of the TM_0 mode: an increase in E_x amplitude simultaneously increases I and decreases C . This anticorrelation is stronger at longer wavelengths due to the reduced damping of the TM_0 mode in that region of the spectrum. Retardation effects at shorter wavelengths (< 610 nm) favor the excitation of $\text{HE}_{\pm 1}$ modes, which contribute primarily to the transverse components E_y and E_z such that C and I are correlated at shorter wavelengths. In addition, it should be noted that modifying the geometry of the ends of the nanowire provides an additional strategy for tuning the in- and out-coupling efficiency of each excited SPP mode, and thus offers additional options for designing various sub-wavelength circularly polarized light sources.

The implementation of a broadband, subwavelength linear-to-circular polarization converter is highly desirable for numerous nanophotonics applications. Particularly, we envisage the realization of a metallic nanowire-based circularly polarized photon source as a unique new type of tip for scanning near-field optical microscopy [17] or tip-enhanced Raman spectroscopy. It is quite likely that single chiral molecule or “artificial molecule”-light interactions may be facilitated by this source [2,18]. Other possible

applications include the study of spin dynamics of spintronic materials and subwavelength all-optical magnetic recording [19].

In conclusion, we have shown that chiral SPPs can be excited on metallic nanowires. This is accomplished by illumination of one end of the nanowire with linearly polarized light at a nominal 45° polarization angle with respect to the nanowire axis. Photons emitted from the end of the nanowire when excited in this manner can be highly circularly polarized, making this structure a broadband, subwavelength linear-to-circular polarization converter. This discovery of chiral electromagnetic surface waves creates new opportunities for the design of nanoscale integrated photonic components, and provides a subwavelength circularly polarized light source that may be useful as a local probe of enantiomeric molecules and other reduced-symmetry nanoscale systems.

This work was supported by NSFC Grants (Nos. 10874233 and 11004237), MOST Grants (Nos. 2006DFB02020 and 2009CB930700), “Knowledge Innovation Project” (KJ CX2-EW-W04) of CAS, the Robert A. Welch Foundation under grants C-1220 (N.J.H.) and C-1222 (P.N.), and the Nanometer Structure Consortium at Lund University, nmC@LU (H. X. X and U. H.).

*hongxingxu@iphy.ac.cn

- [1] L. D. Barron, *Molecular Light Scattering and Optical Activity* (Cambridge University Press, Cambridge, England, 2004); E. Hendry *et al.*, *Nature Nanotech.* **5**, 783 (2010).
- [2] Y. Tang, and A. E. Cohen, *Phys. Rev. Lett.* **104**, 163901 (2010); *Science* **332**, 333 (2011).
- [3] J. K. Gansel *et al.*, *Science* **325**, 1513 (2009); Y. Gorodetski *et al.*, *Phys. Rev. Lett.* **101**, 043903 (2008); Z. Fan, and A. O. Govorov, *Nano Lett.* **10**, 2580 (2010); M. Liu *et al.*, *Nature Nanotech.* **5**, 570 (2010); A. I. Fernandez-Dominguez *et al.*, *Appl. Phys. Lett.* **93**, 141109 (2008).
- [4] D. K. Gramotnev, and S. I. Bozhevolnyi, *Nat. Photon.* **4**, 83 (2010); W. L. Barnes, A. Dereux, and T. W. Ebbesen, *Nature (London)* **424**, 824 (2003).
- [5] A. V. Akimov *et al.*, *Nature (London)* **450**, 402 (2007); D. E. Chang *et al.*, *Phys. Rev. Lett.* **97**, 053002 (2006); H. Wei *et al.*, *Nano Lett.* **9**, 4168 (2009).
- [6] D. E. Chang *et al.*, *Phys. Rev. B* **76**, 035420 (2007).
- [7] H. Ditlbacher *et al.*, *Phys. Rev. Lett.* **95**, 257403 (2005); M. Allione *et al.*, *Nano Lett.* **8**, 31 (2008).
- [8] Z. P. Li *et al.*, *Nano Lett.* **9**, 4383 (2009); T. Shegai *et al.*, *Nano Lett.* **11**, 706 (2011).
- [9] Y. R. Fang *et al.*, *Nano Lett.* **10**, 1950 (2010); Z. P. Li *et al.*, *Small* **7**, 593 (2011).
- [10] H. Wei *et al.*, *Nano Lett.* **11**, 471 (2011).
- [11] C. A. Pfeiffer, E. N. Economou, and K. L. Ngai, *Phys. Rev. B* **10**, 3038 (1974).
- [12] L. Novotny and C. Hafner, *Phys. Rev. E* **50**, 4094 (1994).

-
- [13] P. B. Johnson and R. W. Christy, *Phys. Rev. B* **6**, 4370 (1972).
[14] F. Hao *et al.*, *Chem. Phys. Lett.* **458**, 262 (2008).
[15] All incident phases give similar results: for this specific incident phase the three excited components appear more equivalent.
- [16] P. Biagioni *et al.*, *Phys. Rev. Lett.* **102**, 256801 (2009).
[17] M. Schnell *et al.*, *Nano Lett.* **10**, 3524 (2010).
[18] S. Kühn *et al.*, *Phys. Rev. Lett.* **97**, 017402 (2006).
[19] C. Stanciu *et al.*, *Phys. Rev. Lett.* **99**, 047601 (2007).